Valence band and core-level photoemission of Au/Ge(001): Band mapping and bonding sites

S. Meyer,[1] L. Dudy,[1] J. Schäfer,[1] C. Blumenstein,[1] P. Höpfner,[1] T. E. Umbach,[1] A. Dollinger,[1] X. Y. Cui,[2] L. Patthey,[2] and R. Claessen[1]

[1]*Physikalisches Institut und Röntgen Center for Complex Materials Systems, Universität Würzburg, D-97074 Würzburg, Germany*

[2]*Swiss Light Source, Paul Scherrer Institut, CH-5232 Villigen, Switzerland*

(Received 15 November 2013; revised manuscript received 26 August 2014; published 8 September 2014)

We have used photoemission spectroscopy in order to investigate the electronic states and chemical bonding related to Au induced atomic chains on the Ge(001) surface. Angle-resolved photoemission reveals two types of dispersions around the Fermi level whose intensities strongly depend on the incident photon energy. Around $h\nu = 100$ eV, the band structure is dominated by an electronlike band of mainly one-dimensional (1D) character, which shows Tomonaga-Luttinger-like power-law behavior in the k-integrated spectral function. In contrast, lower photon energies reveal a metallic holelike dispersion which resembles the Ge bulk structure with its heavy-hole, light-hole, and split-off branches. The Au $4f$ core-level spectra show two doublets indicating two different Au bonding sites, whereas the Ge $3d$ core-level shows two surface components and one bulk component.

DOI: 10.1103/PhysRevB.90.125409 PACS number(s): 71.20.−b, 71.27.+a, 71.30.+h, 79.60.−i

I. INTRODUCTION

Unlike conventional three-dimensional electronic systems, electronic ground states in reduced dimension are predicted to deviate from the widely applicable canonical quasiparticle picture. In case of a metallic (quasi-) one-dimensional (1D) chain, for example, there are typically two kinds of ground states discussed. For the first one, finite coupling to phonons causes a metal-insulator-transition accompanied by a periodic lattice distortion. This is the well-known Peierls instability [1,2]. In contrast to this, there is the possibility that, within a certain energy regime, a stable 1D metallic state can be found. The theoretical framework is the Tomonaga-Luttinger liquid (TLL) where quasiparticles do not exist anymore but, instead, there are collective bosonic excitations of spin and charge [3,4]. A spectroscopic fingerprint of this spin-charge separation is the power-law behavior of the low-energy density of states, E^{α} with the nonuniversal exponent α. Another fingerprint (visible for $\alpha < 0.5$) is the observation of two dispersive peaks in the one-particle spectral function related to the phenomenon of spin-charge separation. For $\alpha > 0.5$, the spin excitation is reduced to a broad peakless hump, leaving only one sharp peak for the charge-excitation.

A promising material class suitable to study these exotic states of matter are atomic chains, where metal atoms self-assemble on semiconductor surfaces. Two examples, both of which have been extensively discussed in terms of a Peierls instability, are indium on Si(111) and gold on Si(553)/(557) [5]. Regarding the TLL phase, the only substantial experimental evidence for a TLL phase in atomic chains on semiconductor surfaces has so far been provided for Au chains on Ge(001) [6–8]. Although a phase transition of the $p(4 \times 1)$ superstructure was found at elevated temperatures of 585 K [9], the basic $c(8 \times 2)$ structure and its concomitant electronic states remain stable even down to 10 K [10]. These electronic states form a small electron pocket below the Fermi level [8,11], which is of significant 1D character [10], at least near the chemical potential [12]. The direction of the conduction path as compared to the chain direction in real space is still under debate [10–12]. Nevertheless, the low-energy behavior of the density of states is known to be characterized by a power-law suppression which was observed by scanning tunneling spectroscopy as well as by angle-resolved photoemission (ARPES) [6] and complies with the theoretical predictions for a TLL state [3,4].

However, previous ARPES studies were restricted either to low ($h\nu \leqslant 35$ eV) [6,11,12] or high photon energies ($h\nu = 100$ eV) [10], which still bears some uncertainties about the correct description of the band structure due to cross-section or matrix element effects. Furthermore, only little is known about the underlying atomic structure [7,13], thereby preventing a theoretical modeling of this system.

The present report attempts to complete the picture of the electronic states in Au/Ge(001) by inspecting the electronic band structure in great detail. The aim is threefold. (i) A full account of the valence bands, going beyond the more well-known 1D features, (ii) a temperature-dependent inspection of the previously noted Tomonaga-Luttinger behavior, and (iii) a record of the core levels relating to Ge and Au, respectively, so as to derive information about the Au coverage at the surface, and to thus provide guidance for the still sought-after atomic structure model.

We therefore start out to disentangle the character of the 1D band from the remaining valence bands. In this study, we use a range of photon energies up to 100 eV to tune the cross sections, and to check in which of the bands perpendicular dispersion behavior can be found. This ultimately leads to the assignment of a metallic (Fermi-Dirac-like) interface state, which bears resemblance to Ge bulk states, yet lacks three-dimensional dispersion. Secondly, we perform a line shape analysis of the leading edge of the 1D band, from $T = 10$ to 120 K. The observed power-law depression of the TLL spectral weight towards the chemical potential is, within error bars, not dependent on temperature, which is consistent with the absence of any lattice distortions. Thirdly, regarding the core-level analysis (Au $4f$, Ge $3d$), we find indication for more than one bonding site for the Au atoms. The implications for a structural model, the possibilities for which are considerably narrowed by our findings, are discussed.

II. EXPERIMENTAL

N-type doped planar Ge(001) substrates were chemically etched and oxidized as described in Ref. [14]. *In situ* preparation was performed in an ultrahigh vacuum chamber with a base pressure of 1×10^{-10} mbar located at the surface and interface spectroscopy (SIS) undulator beamline of the Swiss Light Source. Gold was evaporated on substrates held at $T = 650$ K. The correct phase, determined by the $c(8 \times 2)$ reconstruction with its additional $p(4 \times 1)$ superstructure, as well as good long-range order and complete surface coverage was verified by low-energy electron diffraction (LEED). The total amount of gold is assumed to be 0.75 monolayers (ML) according to Gallagher and co-workers [15]. The photoemission data were obtained using a Scienta R4000 analyzer and a six-axis goniometer allowing access to all directions in k space. The polarization was right-handed circular. The angle of incident between the incoming light and the analyzer was 45°. If not stated otherwise, the temperature was set to 50 K. The total energy resolution was set to ~15 meV. Core-level spectra were taken at $h\nu = 130$ eV in the angle-integrated mode.

III. RESULTS AND DISCUSSION

A. Band features

Due to the intrinsic dual-domain nature of planar Ge substrates [16], where the dimers already form chainlike rows, the gold-induced chains align in parallel but switch their orientation by 90° going across a single-height terrace step, see the scanning tunneling microscope (STM) topographic images on left side of Fig. 1 ($U = +0.8V$). The unit cell of the Au-Ge(001) structure can be described as $c(8 \times 2)$, and in addition there is a long-range ordering, which leads to a complex superstructure, which is described in detail in Ref. [9]. The latter may be denoted in short-hand notation as "$p(4 \times 1)$" if understood to operate on the individual unit cells. As the $c(8 \times 2)$ is the smallest real-space unit and, therefore, has the largest repetition unit in reciprocal space, we want to relate our measurements in the following to the $c(8 \times 2)$. The resulting orientations of the $c(8 \times 2)$ surface Brillouin zones (SBZ's) are depicted on the right side of Fig. 1.

First, we discuss the band maps (the intensity of the photoelectrons as a function of binding energy and momentum) that were recorded under variation of the photon energy and are depicted in Fig. 2. Darker color means higher intensity. We expect two effects when tuning the photon energy: (i) a change of the probed momentum of the electrons inside the specimen along the surface normal ($k_\perp$). This effect should be of minor importance since we deal with a surface structure. (ii) A change in the relative intensities of the probed excitations due to photon energy dependent transition matrix elements. We expect the latter to be more important since the photon energy will be tuned within a relatively large range (25 to 100 eV) with different orbitals being involved, mostly Au 5*d* and 6*s* as well as Ge 4*s* and 4*p*.

We start with the measurements at photon energies of $h\nu = 100$ eV as shown in Fig. 2(a). The data were recorded along the path indicated in the SBZ on the inset of Fig. 2(a).

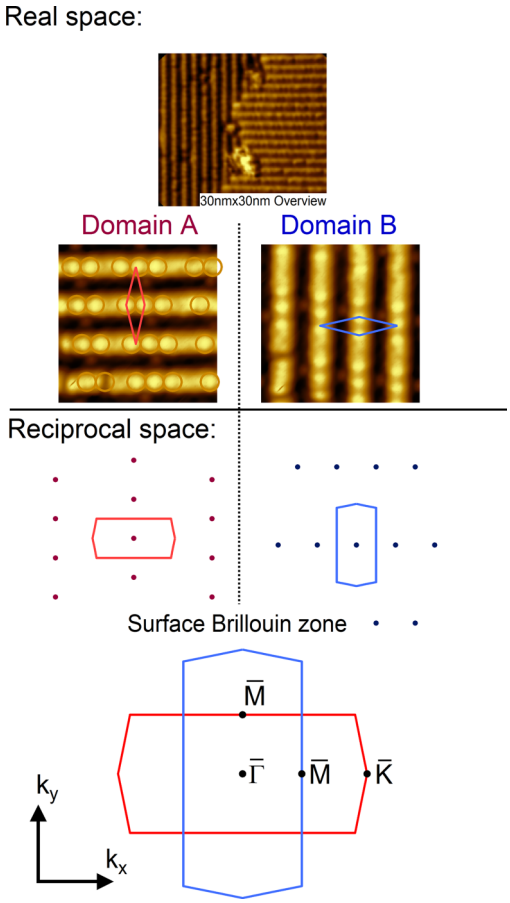

FIG. 1. (Color online) Schematic of both rotational domains A and B of the nanowires in real space and their corresponding reciprocal space pattern. The resulting surface Brillouin zones (SBZ's) are shown on the bottom.

The most prominent features in the intensity distribution close to the Fermi energy are the electron pockets labeled with "1D" and centered about $k_x = \pm 0.2$ Å^{-1}. After changing the photon energy to $h\nu = 55$ eV as shown in Fig. 2(b), downward parabolas can be found at $k_x = 0$ and ± 0.4 Å^{-1}. They show a splitting into a light-hole (LH) branch at E_F and a split-off (SO) branch at $E_B = -0.3$ eV . Both branches match the expected bulk Ge valence band [17] with the LH branch being cut slightly below its top as in a heavy p-type doping scenario. Notably, none of the above band maps shows such clear indications of the heavy-hole (HH) band. Data with this feature much clearly visible will be discussed later. The fact that the valence band maximum is located quite near the Fermi level—despite the strong n-type doping of the substrate—is attributed to a Schottky barrier situation, with the Fermi level pinned by the high density of the Au-induced surface states and hence causing the Ge VB bending to lower binding energies. The Schottky barrier heights for Au-electrodes on n-type Ge(001) are around 0.6 eV [18]. This value compares well with photoelectron studies of Au deposited on the n-type Ge(001)-2×1 surface seeing a reduction of the Au $4f$ binding energy of around 0.6 eV when going from 1ML coverage to high coverage [19]. Keeping in mind that the Ge

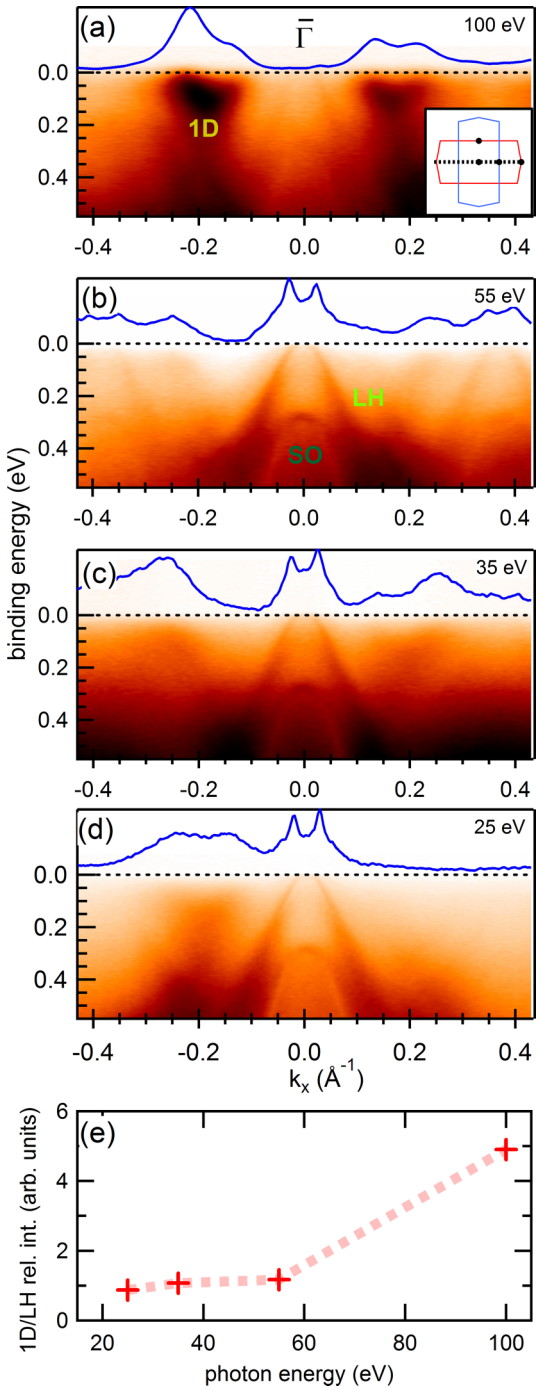

FIG. 2. (Color online) ARPES band maps for various photon energies measures at (a) $h\nu = 100$, (b) 55, (c) 35, and (d) 25 eV . The intensity ratio of electron pocket (1D) and light-hole (LH) band changes significantly, favoring the electron pocket at high, the hole band at intermediate photon energies. For lower photon energies, the split-off (SO) band is discernible as well. The blue curve on the top of each band map shows the MDC at $E_B = 30$ meV. (e) Relative intensity ratio of electron pocket and light-hole band as a function of photon energy.

bulk band gap is ≈0.7eV this is consistent with our above observation.

A further decrease of the photon energy to $h\nu = 35$ eV in Fig. 2(c) causes a loss of the symmetric appearance of the 1D electron pockets at negative k values compared to the one shown for higher photon energies. This loss in symmetry can be best seen when looking at the momentum distribution curve (MDC) of the photoelectron intensity at a constant binding energy as displayed in Fig. 2. Here, the binding energy was set to 30 meV like the integration window. At $h\nu = 25$ eV, the electron pocket, which is located to the right of the $\bar{\Gamma}$ point, disappears, while its counterpart on the left-hand side becomes more symmetric compared to $h\nu = 35$ eV .

One may note that both the electron pocket as well as the hole state provide no evidence for any $k_\perp$ dispersion, as would be naively expected for typical bulk bands when the photon energy is changed. One explanation of this behavior might be that the observation of the bulk dispersion is experimentally obscured. An apparent $k_\perp$ independence would then be attributed to the limited escape depth λ of the photoelectrons in that photon energy range. This finite λ causes the photoemission signal of the bulk band structure to be broadened by a Gaussian with a width of $\Delta k_\perp \propto 1/\lambda$ (where $k_\perp$ is the direction perpendicular to the surface) [20,21]. This will effectively lead to the observation of the surface projection of the bulk three-dimensional electronic structure, making it difficult to distinguish it from a 2D surface state in ARPES. However, contrary to this conjecture, in the past it has been demonstrated that true bulk states of Ge(001) can indeed be clearly discerned in photon energy scans [22].

Since it is already known that because scanning tunneling spectroscopy (STS) detects the 1D state only [6], the hole state must reside at deeper layers. It must therefore seem more plausible that this state has to be specified as an interface state [10] or, equivalently, a subsurface state, which is of intermediate character between a bulk state and surface state. Indeed, for metal-adsorbed germanium surfaces, such interface states extending several layers below the surface have been reported earlier [23–25]. In particular, in a recent study by Ohtsubo *et al.* [26] these subsurface states have been analyzed in detail for Ge(111) substrates which are reconstructed with metal adatoms. Such two-dimensional states are localized in subsurface regions of the substrate, as is reproduced by density-functional theory calculations. Both band dispersion and orbital character of these states are derived from the bulk heavy-hole, light-hole, and spin-orbit split-off bands, respectively. This indicates an origin of the subsurface states from the bulk bands as a result of the perturbed crystal periodicity due to the interface with the metal adlayer. Such scenario is also consistent with the present case, which refers to a (001) surface rather than the previous observations on (111) surfaces with planar surface reconstructions. It was thus not *a priori* clear whether or not a subsurface state would develop at all, and in particular, whether or not it is following the 1D character of the adsorbed nanowires or, alternatively, showing a 2D-like nature (as observed). It is therefore noteworthy that the interface state develops independent of the 1D surface reconstruction. Since the holelike state is likely originating from Ge orbitals, one explanation for its metallic behavior might be charge transfer from Ge to Au at the interface. Here, Au would act as acceptor (p-type doping), lowering the Fermi level into the formerly insulating Ge valence band.

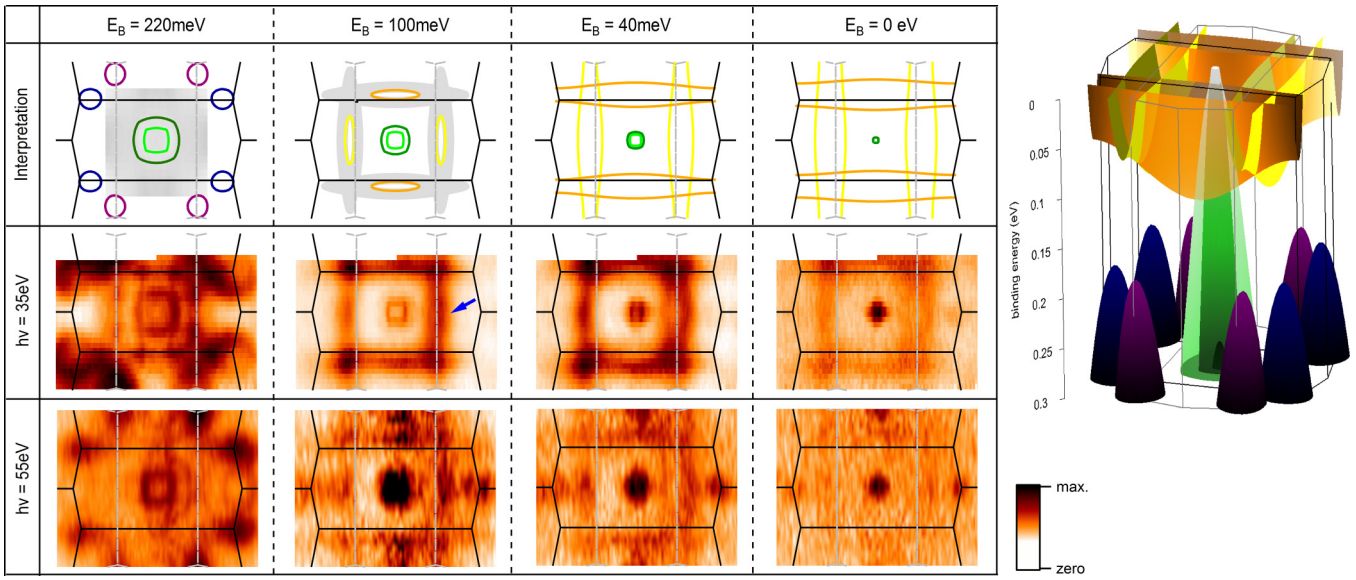

FIG. 3. (Color online) Constant energy surfaces at various interesting binding energies for photon energies of $h\nu = 55$ and 35 eV . The interpretation of the features is depicted in the upper row and in the three dimensional schematic on the right. The interpretation structure sketched to scale: electron pocket in yellow with small degree of lateral coupling; Ge heavy-hole, light-hole, and split-off bands in green, and the so-called garland bands in blue/purple.

The qualitative intensity ratio of electron pocket and LH band is presented in Fig. 2(e). Here we use the intensity at the band bottom of the 1D band at $k_x = 0.2$ Å^{-1} compared to the intensity of light-hole band at the same binding energy. Besides the intensity drop of the electron pocket for lower photon energies, one notices an almost 1:1 ratio at $h\nu = 35$ eV, which will be used later on for the line-shape analysis.

B. Dimensionalities and periodicities

In the following both states, electron pocket and light-hole, are analyzed for their dimensionality and periodicity from constant energy surfaces (CES). These CES's display the intensity of the photoelectrons as a function of the 2D (in-plane) momentum, i.e., the CES at zero binding energy represents the Fermi surface. Here we focus on two different photon energies, $h\nu = 55$ and 35 eV, which allow the observation of the hole state. The CES's at interesting binding energies are depicted in Fig. 3. Above the CEF's, we displayed our interpretation of the dispersion. This interpretation is based on an extraction of the maxima in energy direction (EDC) and momentum direction (MDC) of the photoemission signal. Our interpretation of the CES's on the top of Fig. 3 represents constant energy contours of the three dimensional schematic on the right of Fig. 3 and is meant to correctly reflect the energy and momentum scale.

Focussing on the CES's and starting hat the Fermi energy ($E_B = 0$ eV), we notice a small pointlike shape in the center of the Brillouin zone which is produced the hole-paraboloid (see green cone in the right side of Fig. 3). The electron pockets can be seen much clearer at $h\nu = 35$ eV compared to $h\nu = 55$ eV . There one sees a squarelike shape. Considering that the square shape results from the superposition of the two rotational domains, one clearly notices that the dispersion of the electron pocket is *more 1D than 2D* [10,12]. That is because for a perfect 2D electron pocket, the dispersion would resemble the one of a paraboloid, therefore producing circlelike shapes in the CES's. For a perfect 1D electron pocket, one would have only one dispersive direction and, therefore, in simplest consideration, the dispersion would merely have the shape of a half-pipe. In the CES's then, a doublet of parallel lines running along the nondispersive direction would be produced. Considering now two electron pockets per domain (one domain causing a left and a right vertical doublet, the other domain causing up/down horizontal doublets), this explains the square shape look at the CES's at $E_B = 0$ and 40 meV.

Let us now discuss the CES's at $E_B = 100$ meV. Compared to $E_B = 40$ meV, we notice an intensity increase in the middle of the electron pockets. That increase is best visible at $h\nu = 35$ eV in the right of the vertical electron pockets (see arrow). In our interpretation sketch, this intensity has to be compared with the yellow ovals and represents the bottom of the electron pockets (compare also with Fig. 2 at $h\nu = 100$ eV). In the experimental CES's for $E_B = 100$ meV, one also notices a squarelike shape and four intense dots at the corners of the square. As ARPES is measuring the spectral function and not just a dispersion, these features are caused by the lifetime broadening (in case of quasiparticles, self-energy) which, in principle, adds intensity from other energies. In order to illustrate that in our interpretation sketch (at $E_B = 100$ meV), we show the grey region, which is our determined dispersion relation $E(k)$ displayed for the energy interval between $E_B = 60$ meV and 100 meV. One sees nicely that the grey shaded area fits well with the squarelike shape and one can imagine that, at the overlapping region at the corners, both the domains will add up to the intense dots. Coming back to the dimensionality of the electron pocket, our interpretation that the bottom of the electron pockets is a (yellow) oval

determines the degree of one dimensionality. When using k_y for the non-1D direction, the dispersion component is roughly $E(k_y) \sim t_\perp \cos(k_y)$ with the upper bound of the perpendicular hopping being $t_\perp \leqslant 25$ meV.

Evidence for a heavy-hole branch is found at binding energies below the band bottom of the electron pockets, see $E_B = -0.22$ eV in Fig. 3. Here the former central pointlike shape splits into two circles which can be related to light and heavy holes. Thus the dimensionality of these states is at least two-dimensional, if not a three dimensionality is hidden by the above mentioned $\Delta k_\perp$ broadening. At $E_B = -0.22$ eV, beside the LH and HH, there are some other features visible near the BZ center which region we show in our interpretation sketch (for $E_B = -0.22$ eV) as a grey area. As these features look different for $h\nu = 55$ eV (flowerlike shape) and $h\nu = 35$ eV (squarish shape), we assume that these features most likely have its origin in the bulk electronic structure.

At the corner of the Brillouin zone additional circular shapes appear at $k_{(x/y)} = \pm 0.2/\pm 0.4$ Å^{-1}. They are related to fully occupied bands at the zone boundary, which will be called "garland band" (GB) in the following. The evolution of this band as well as the heavy-hole branch can be observed in band maps as a function of k_y. The central cut through the SBZ, i.e., $k_y = 0$ Å^{-1} at $h\nu = 55$ eV in Fig. 4(a), already contains a hint of the heavy hole at higher binding energies right below the electron pocket (marked by an arrow and HH). There is also already a weak shadow visible around the LH. It gets more pronounced for $k_y = 0.1$ Å^{-1} in Fig. 4(b), where a crossing of two neighboring heavy-hole bands is visible. If the band map cut is taken along the SBZ boundary, see Fig. 4(c), the garland band shows up with its top located at $k_x = 0.4$ Å^{-1} and $E_B \sim -0.22$ eV . A complete three-dimensional sketch of the band structure in the near E_F region is given in Fig. 3(b).

Keeping in mind the additional $p(4 \times 1)$ superstructure observed in LEED, one may ask whether the band structure is affected by this symmetry. Let us again mention that scanning tunneling microscopy has shown that the combination of $c(8 \times 2)$ and $p(4 \times 1)$ superstructure causes a larger real space unit cell [9], which on the other hand results in a smaller unit cell in reciprocal space. Here we have to state that no evidence of backfolding due to other Brillouin zones than the $c(8 \times 2)$ is observed.

C. Line-shape analysis

As judged from the afore presented band structure, Au/Ge(001) exhibits *two metallic states* (1D electron pocket and 2D/3D hole state), where metallic means these states cross the Fermi energy. An explicit proof for the separation of both states in momentum can be obtained from Figs. 5(a) and 5(b) recorded at the favored photon energy of $h\nu = 35$ eV, where both states have equal intensity. Here one clearly notices that the band bottom of the 1D electron pocket is located well above the heavy-hole branch. Thus a more refined analysis on the electronic ground state can be performed based on the inspection of the k-integrated spectral function in the low-energy range.

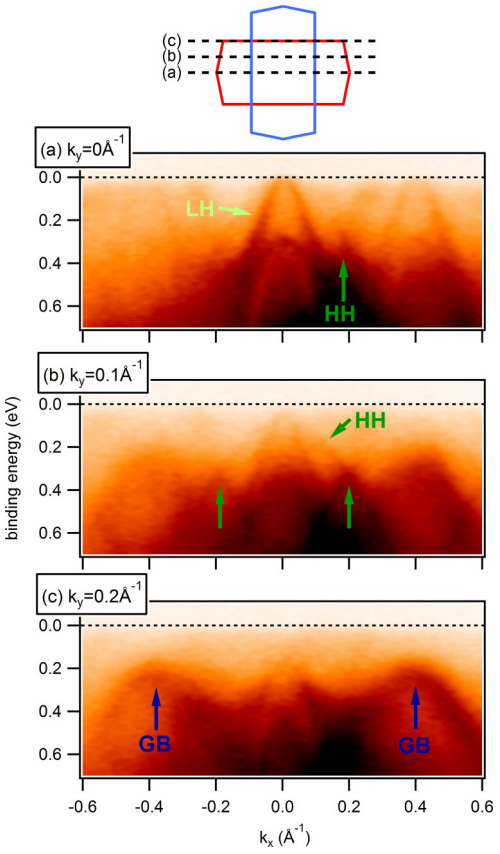

FIG. 4. (Color online) Band map taken at $h\nu = 55$ eV as a function of k_y. (a) Already at $k_y = 0$ Å^{-1} beside the LH, the HH can be observed as a weak shadow around the LH and a crossing point of two neighboring HH branches (arrows). These evolve HH-branches with increasing k_y, as for (b) $k_y = 0.1$ Å^{-1}. (c) The garland band (GB) appears at at the zone boundary $k_y = 0.2$ Å^{-1} at $k_x = 0.4$ with its top at $E_B = -0.22$ eV marked by blue arrows.

The integration areas are indicated by black frames in Fig. 5(a). Starting with the 2D/3D hole state, we notice a nice accordance of the k-integrated line shape with a Fermi distribution, solid blue line in Fig. 5(c), as expected for a typical metallic state. Its width amounts to 14 meV in good agreement with the applied temperature ($T = 10$ K) and energy resolution ($\Delta E = 15$ meV). Notably, the position of the Fermi energy is not affected by increasing temperature or the photon flux in terms of surface photo voltage. Hence, the 2D hole state serves as an intrinsic and reliable reference for the Fermi energy.

Figure 5(b) gives us confidence us that there is no intensity from the heavy-hole branch leaking into the k-integrated area of the 1D-pocket. Turning to the line shape of the 1D electron pocket in Fig. 5(d), we observe a suppression of spectral weight towards the Fermi level. This behavior is characteristic of a TLL state, where the density of states approximately follows a power law in energy with the anomalous exponent α. From previous experiments [6], the exponent of Au/Ge(001)is known to exceed 0.5, which prevents the observation of spin-charge separation in that sense that the spinon feature is broad [27]. Thus we concentrate on the k-integrated line shape, which

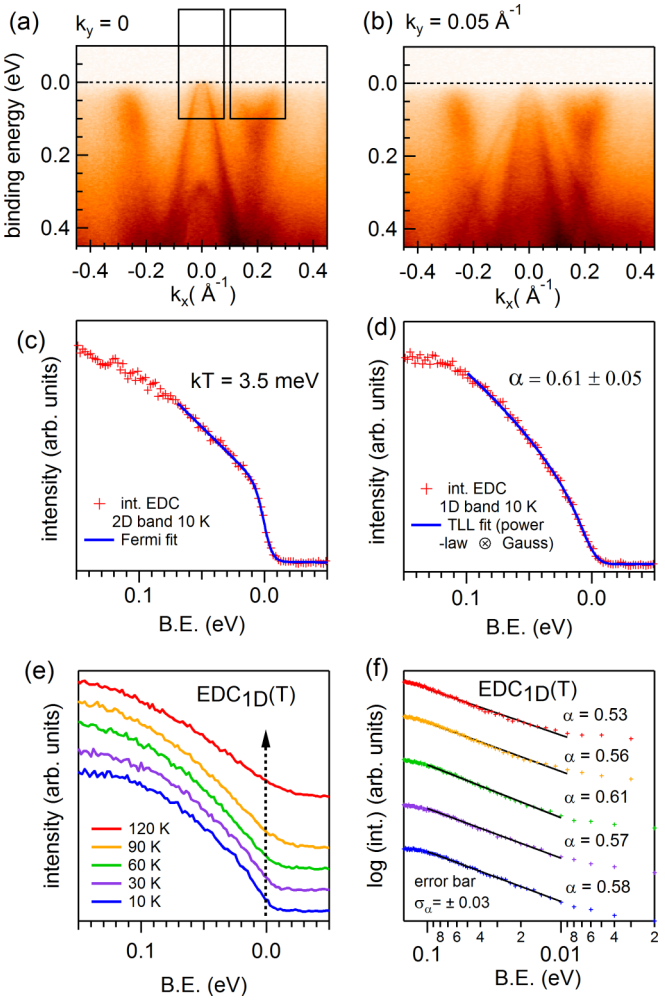

FIG. 5. (Color online) (a) Band map at $h\nu = 35$ eV along main axes of the SBZ. Integration areas are marked by black boxes. (b) Band map at $k_y = 0.05$ Å^{-1} that shows the clear separation of heavy-hole branch and 1D electron pocket. (c) Band integrated line shape (markers) for the 2D interface states at 10 K resembling a metallic Fermi distribution (solid fit line). (d) Integrated line shape of the 1D band (markers). A TLL power-law convolved with a Gaussian function yields a TLL exponent of $\alpha = 0.61$ (solid line). (e) Temperature series of the k-integrated line shape of the 1D band. The spectra have been offset vertically. (f) Double logarithmic presentation of (e) with linear fit. The TLL exponent, i.e., the slope, stays almost constant in temperature.

is a good approximation of the density of states. Our power-law fit includes a convolution with a Gaussian distribution to account for a finite temperature and energy resolution. At the lowest available temperature of 10 K the exponent yields $\alpha = 0.61 \pm 0.05$, see Fig. 5(d). Increasing temperatures do not affect the spectra significantly, see Fig. 5(e), where a subtle change is only observed at 120 K.

A common procedure with less fitting parameters but an assumption of zero temperature is a double-logarithmic plot of the data [28,29]. Here the exponent can be extracted from the slope of a linear fit. We limit ourself here to the energy scale of E_B from 100 to 10 meV.

In the present case of Au/Ge(001), the exponent stays more or less constant up to 120 K, see Fig. 5(f), with an average value of 0.57. A temperature scaling of a TLL exponent was reported recently for the paradigmatic TLL system $Li_{0.9}Mo_6O_{17}$. Primary reports of $\alpha = 0.9$ at room temperature [30] were refined later on, yielding values of $\alpha \sim 0.6$ for decreasing temperatures [31,32]. Such a temperature dependence of α cannot be explained within the TLL theory but requires either a possible interaction of the charge and spin channels of two bands merging at E_F, or short-range interactions induced by disorder for a non-half-filled system [33,34]. No evidence for such a thermal renormalization can be found within error bars in the present study of Au/Ge(001).

The slight increase of the TLL exponent compared to our previous study of 0.53 [6] is most likely due to the sample imperfection. Since the photon spot is typically in the order of 50–100 μm, ARPES averages over several wire terraces (common size of 200×200 nm^2). Thus both the natural limitations, i.e., the finite wire length caused by terrace steps or defects (vacancies, adatoms), and extrinsic effects like adsorption of residual gas may apply here. Any defect limiting the chain length may act as a scattering center, which will enhance the TLL exponent locally. This argument is supported by scanning tunneling spectroscopy (STS), which as a real-space technique locally extracts the TLL exponent. Chain ends inspected with STS yield an increase from the bulk $\alpha_{\mathrm{bulk}(STS)} = 0.53$ to $\alpha_{\mathrm{boundary}(STS)} = 1.2$ [6]. Reconsidering the relatively large averaging area of ARPES compared to STS, the current experimental exponent $\alpha_{\mathrm{ARPES}} = 0.57$ can be understood as an intermixture of both $\alpha_{\mathrm{bulk}(STS)}$ and $\alpha_{\mathrm{boundary}(STS)}$.

Another important insight warrants mentioning, namely the observation of the 2D-like metallic interface state in close k-space vicinity to the 1D TLL state. Specifically, for both spin and charge excitations, respectively, the power-laws depend on the effective Coulomb correlation in the charge sector, see, e.g., Ref. [35]. It must be assumed, unlike in a free-standing atomic chain, that the effective Coulomb interaction will be reduced due to the presence of the metallic state, and the resulting exponent α may be modified compared to a hypothetical "bare" situation.

D. Chemical environment from core-level spectroscopy

In order to study the chemical environment of the Ge and Au atoms, we performed core-level spectroscopy at $h\nu = 130$ eV for the Ge $3d$ and Au $4f$ states. The analytical power of the core-level analysis for structural modeling was already proven for the bare c(4 × 2)-reconstructed Ge(001) surface by Erikson and Uhrberg [36]. They deconvolved the Ge(001) $3d$ core level using five Voigt doublets which accounted for the different bulk and surface contributions, including the two different dimer configurations "up" and "down." With their fitting parameters as guidelines, the same analysis is carried out here for Ge in Au/Ge(001).

The fit was performed with a Lorentzian width (LW) of 0.15 eV, a spin-orbit splitting of $\Delta_{\mathrm{SO}} = 0.59$ eV and a branching ratio ($d_{3/2} : d_{5/2}$) between 0.65 and 0.7. The peak position, amplitude and Gaussian width were free fitting parameters to allow for convergence of the fit. For Ge $3d$,

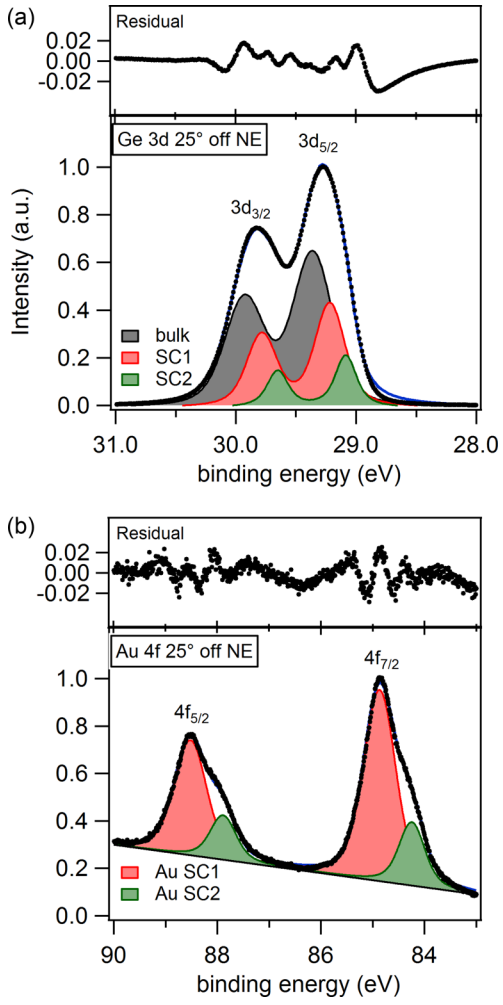

FIG. 6. (Color online) (a) Ge $3d$ core level of reconstructed Au/Ge(001) recorded at $h\nu = 130$ eV, 25° off normal emission (NE). One bulk and two surface components (SC 1 and 2) are found. (b) Au $4f$ core level of Au/Ge(001) showing a distinct two-peak structure that indicates two inequivalent Au sites. The upper panels show the residuals of the corresponding peak fits.

three Voigt doublets are sufficient to get a good match to the experiment, see Fig. 6(a). The upper panel show the residual of the fit, indicating only weak deviations.

According to the initial model proposed by Erikson and Uhrberg, the three components found in Ge $3d$ of Au/Ge(001) represent the bulk ($E_B = -29.3$ eV), a relaxed or reconstructed surface layer (surface component SC 1 at $E_B = -29.15$ eV) and another surface component (SC 2 at $E_B = -29$ eV), respectively. The three doublets match the previous results by Niikura and co-workers for the Ge $3d$ core level of Au/Ge(001) [37].

The corresponding Au $4f$ (spin-orbit split) core level is shown in Fig. 6(b), with a clear twofold substructure which can be modelled by *two* Voigt doublets ($LW = 0.25$ eV, $\Delta_{SO} = 3.65$ eV), thus indicating *two* inequivalent bonding sites for Au. The intensity ratio between the two doublets is close to 3:1, which accounts in a direct interpretation either to four Au atoms (0.5 ML) or eight Au atoms (1 ML) per unit cell with eight Ge atoms underneath.

Interestingly, Gallagher *et al.* claim a precise determination of 0.75 ML [15], which corresponds to six Au atoms per $c(8 \times 2)$ unit cell and, in case of two components as observed in experiments, an expected intensity ratio of 2:1. One explanation for the discrepancy in the intensity ratio might be layer dependent damping where Au atoms are located in the reconstruction in different depths below the surface. Another reason might be surplus gold, which segregates into the bulk during the growth procedure [38,39]. Since Gallagher and co-workers do not provide any error bars, our core-level data can be reconciled with 0.75 ML by assuming an uncertainty of 0.25 ML.

A key insight into whether or not the system is in a metallic state may, in principle, be derived from the asymmetry of the core-level line shape (adatoms and substrate atoms alike). This asymmetry is usually attributed to free charge carriers in conventional metals [40]. According to our analysis, the core-level shapes of both Au $4f$ and Ge $3d$ do not exhibit any asymmetry within the experimental uncertainty. How does this compare to other chainlike systems? For atom chains formed by In on Si(111), which are metallic at room temperature and susceptible to a Peierls-like metal-insulator transition, asymmetries have been noted for both In $4d$ and Si $2p$ components, respectively [41], with a reduction of the asymmetric tail upon cooling. Likewise, in Pb on Si(557) near monolayer coverages, asymmetric metallic tails are noted for both Pb $5d$ and Si $2p$ [42]. Yet, the picture becomes more complicated for Au on Si(55 12), where five components are seen for Si $2p$, and two for Au $4f$ [43]. However, despite a metallic character found in the valence band spectra, the authors did not identify asymmetries in the either type of core levels. This illustrates that the many possible bonding environments obscure a tail analysis for individual core levels. In the present Au-Ge(001), obviously the TLL state does not lead to a noticeably modified line shape for the Au levels. Also, the demonstrated metallic 2D subsurface state of Ge character does not show up in the corresponding core level—very probably covered by the very many other Ge atoms that form the semiconducting surface layer as well as the bulk.

IV. CONCLUSION

In summary, a complete band-mapping overview of the electronic states of Au/Ge(001) is given. The band structure is investigated for a wide range of photon energies, from 25 up to 100 eV. We detect two states close to E_F. One is an electron pocket, which is favored at high photon energies, and a hole state which is more pronounced at lower photon energies. Here a splitting of the hole state into light- and heavy-hole branches with the typical split-off band at higher binding energies could be shown. The light-hole/heavy-hole state remains metallic at low temperatures (10 K), whereas the 1D electron pocket exhibits a TLL power-law suppression. Its anomalous exponent α remains almost constant up to 120 K. The slight increase in the exponent compared to previous STS measurements can be well understood from spatial averaging in ARPES. The Ge $3d$ and Au $4f$ core levels strongly support two surface components each, which may provide further stimulus for structural modeling by density functional theory.

ACKNOWLEDGMENTS

The authors gratefully acknowledge financial funding via the European Community's Seventh Framework Programme (FP7/2007-2013) under grant agreement No. 226716 (for ELISA) and technical support by F. Dubi and C. Hess during beamtime at the Swiss Light Source. This work was supported by the Deutsche Forschungsgemeinschaft (FOR 1162, CLA 124/13-2).

[1] G. Grüner, Rev. Mod. Phys. **60**, 1129 (1988).
[2] K. Rossnagel, J. Phys.: Condens. Matter **23**, 213001 (2011).
[3] J. Voit, Rep. Pro. Phys. **58**, 977 (1995).
[4] K. Schönhammer and V. Meden, J. Elec. Spec. Rel. Phenom. **62**, 225 (1993).
[5] P. C. Snijders and H. H. Weitering, Rev. Mod. Phys. **82**, 307 (2010).
[6] C. Blumenstein, J. Schäfer, S. Mietke, S. Meyer, A. Dollinger, M. Lochner, X. Cui, L. Pathhey, and R. Claessen, Nat. Phys. **7**, 776 (2011).
[7] A. van Houselt, M. Fischer, B. Poelsema, and H. J. W. Zandvliet, Phys. Rev. B **78**, 233410 (2008).
[8] J. Schäfer, C. Blumenstein, S. Meyer, M. Wisniewski, and R. Claessen, Phys. Rev. Lett. **101**, 236802 (2008).
[9] C. Blumenstein, J. Schäfer, M. Morresi, S. Mietke, R. Matzdorf, and R. Claessen, Phys. Rev. Lett. **107**, 165702 (2011).
[10] S. Meyer, J. Schäfer, C. Blumenstein, P. Höpfner, A. Bostwick, J. L. McChesney, E. Rotenberg, and R. Claessen, Phys. Rev. B **83**, 121411(R) (2011).
[11] K. Nakatsuji, R. Niikura, Y. Shibata, M. Yamada, T. Iimori, and F. Komori, Phys. Rev. B **80**, 081406 (2009).
[12] K. Nakatsuji, Y. Motomura, R. Niikura, and F. Komori, Phys. Rev. B **84**, 115411 (2011).
[13] S. Meyer, T. E. Umbach, C. Blumenstein, J. Schäfer, R. Claessen, S. Sauer, S. J. Leake, P. R. Willmott, M. Fiedler, and F. Bechstedt, Phys. Rev. B **85**, 235439 (2012).
[14] C. Blumenstein, S. Meyer, A. Ruff, B. Schmid, J. Schäfer, and R. Claessen, J. Chem. Phys. **135**, 064201 (2011).
[15] M. C. Gallagher, S. Melnik, and D. Mahler, Phys. Rev. B **83**, 033302 (2011).
[16] H. Zandvliet, Phys. Rep. **388**, 1 (2003).
[17] K. Nakatsuji, Y. Takagi, F. Komori, H. Kusuhara, and A. Ishii, Phys. Rev. B **72**, 241308 (2005).
[18] T. Nishimura, K. Kita, and A. Toriumi, Appl. Phys. Lett. **91**, 123123 (2007).
[19] J. Benson, J. Hansen, M. McEllistrem, W. Clendening, and J. Tobin, Surface Sci. **193**, L37 (1988).
[20] V. Strocov, J. Electron Spectrosc. Relat. Phenom. **130**, 65 (2003).
[21] P. J. Feibelman and D. E. Eastman, Phys. Rev. B **10**, 4932 (1974).
[22] A. L. Wachs, T. Miller, T. C. Hsieh, A. P. Shapiro, and T.-C. Chiang, Phys. Rev. B **32**, 2326 (1985).
[23] S.-J. Tang, T.-R. Chang, C.-C. Huang, C.-Y. Lee, C.-M. Cheng, K.-D. Tsuei, H.-T. Jeng, and C.-Y. Mou, Phys. Rev. B **81**, 245406 (2010).
[24] C.-H. Lin, T.-R. Chang, R.-Y. Liu, C.-M. Cheng, K.-D. Tsuei, H. T. Jeng, C.-Y. Mou, I. Matsuda, and S. J. Tang, New J. Phys. **16**, 045003 (2014).
[25] Y. Ohtsubo, S. Hatta, K. Yaji, H. Okuyama, K. Miyamoto, T. Okuda, A. Kimura, H. Namatame, M. Taniguchi, and T. Aruga, Phys. Rev. B **82**, 201307 (2010).
[26] Y. Ohtsubo, K. Yaji, S. Hatta, H. Okuyama, and T. Aruga, Phys. Rev. B **88**, 245310 (2013).
[27] J. Voit, J. Elec. Spectros. Rel. Phenom. **117**, 469 (2001).
[28] H. Ishii, H. Kataura, H. Shiozawa, H. Yoshioka, H. Otsubo, Y. Takayama, T. Miyahara, S. Suzuki, Y. Achiba, M. Nakatake *et al.*, Nature (London) **426**, 540 (2003).
[29] H. Rauf, T. Pichler, M. Knupfer, J. Fink, and H. Kataura, Phys. Rev. Lett. **93**, 096805 (2004).
[30] J. D. Denlinger, G.-H. Gweon, J. W. Allen, C. G. Olson, J. Marcus, C. Schlenker, and L.-S. Hsu, Phys. Rev. Lett. **82**, 2540 (1999).
[31] J. Hager, R. Matzdorf, J. He, R. Jin, D. Mandrus, M. A. Cazalilla, and E. W. Plummer, Phys. Rev. Lett. **95**, 186402 (2005).
[32] F. Wang, J. V. Alvarez, S.-K. Mo, J. W. Allen, G.-H. Gweon, J. He, R. Jin, D. Mandrus, and H. Höchst, Phys. Rev. Lett. **96**, 196403 (2006).
[33] F. Wang, J. V. Alvarez, J. W. Allen, S.-K. Mo, J. He, R. Jin, D. Mandrus, and H. Höchst, Phys. Rev. Lett. **103**, 136401 (2009).
[34] L. Dudy, J. Denlinger, J. Allen, F. Wang, J. He, D. Hitchcock, A. Sekiyama, and S. Suga, J. Phys.: Condens. Matter **25**, 014007 (2013).
[35] M. Guigou, T. Martin, and A. Crépieux, Phys. Rev. B **80**, 045420 (2009).
[36] P. E. J. Eriksson and R. I. G. Uhrberg, Phys. Rev. B **81**, 125443 (2010).
[37] R. Niikura, K. Nakatsuji, and F. Komori, Phys. Rev. B **83**, 035311 (2011).
[38] J. Wang, M. Li, and E. I. Altman, Phys. Rev. B **70**, 233312 (2004).
[39] J. Wang, M. Li, and E. Altman, Surf. Sci. **596**, 126 (2005).
[40] S. Doniach and M. Sunjic, J. Phys. C: Sol. St. Phys. **3**, 285 (1970).
[41] H. W. Yeom, K. Horikoshi, H. M. Zhang, K. Ono, and R. I. G. Uhrberg, Phys. Rev. B **65**, 241307 (2002).
[42] K. S. Kim, W. H. Choi, and H. W. Yeom, Phys. Rev. B **75**, 195324 (2007).
[43] J. R. Ahn, W. H. Choi, Y. K. Kim, H. S. Lee, and H. W. Yeom, Phys. Rev. B **68**, 165314 (2003).